

ETHYNYL (C_2H) IN MASSIVE STAR FORMATION: TRACING THE INITIAL CONDITIONS?

H. BEUTHER, D. SEMENOV, TH. HENNING, AND H. LINZ

Max Planck Institute for Astronomy, Königstuhl 17, 69117 Heidelberg, Germany

Received 2007 November 5; accepted 2008 January 18; published 2008 February 1

ABSTRACT

APEX single-dish observations at submillimeter wavelengths toward a sample of massive star-forming regions reveal that C_2H is almost omnipresent toward all covered evolutionary stages from infrared dark clouds via high-mass protostellar objects to ultracompact H II regions. High-resolution data from the Submillimeter Array toward one hot-core-like high-mass protostellar object show a shell-like distribution of C_2H with a radius of ~ 9000 AU around the central submillimeter continuum peak position. These observed features are well reproduced by a 1D cloud model with power-law density and temperature distributions and a gas-grain chemical network. The reactive C_2H radical (ethynyl) is abundant from the onset of massive star formation, but later it is rapidly transformed to other molecules in the core center. In the outer cloud regions the abundance of C_2H remains high due to constant replenishment of elemental carbon from CO being dissociated by the interstellar UV photons. We suggest that C_2H may be a molecule well suited to study the initial conditions of massive star formation.

Subject headings: astrochemistry — ISM: abundances — molecular processes — stars: early-type — stars: formation — stars: individual (IRAS 18089–1732)

1. INTRODUCTION

Spectral line surveys have revealed that high-mass star-forming regions are rich reservoirs of molecules from simple diatomic species to complex and larger molecules (e.g., Schilke et al. 1997; Hatchell et al. 1998; Comito et al. 2005; Bisschop et al. 2007). However, there have rarely been studies undertaken to investigate chemical evolution during massive star formation from the earliest evolutionary stages, i.e., from high-mass starless cores (HMSCs) and high-mass cores with embedded low- to intermediate-mass protostars destined to become massive stars, via high-mass protostellar objects (HMPOs), to the final stars that are able to produce ultracompact H II regions (UCHIIs; see Beuther et al. 2007 for a recent description of the evolutionary sequence). The first two evolutionary stages are found within so-called infrared dark clouds (IRDCs). While for low-mass stars the chemical evolution from early molecular freezeout to more evolved protostellar cores is well studied (e.g., Bergin & Langer 1997; Dutrey et al. 1997; Pavlyuchenkov et al. 2006; Jørgensen et al. 2007), it is far from clear whether similar evolutionary patterns are present during massive star formation.

To better understand the chemical evolution of high-mass star-forming regions we initiated a program to investigate the chemical properties from IRDCs to UCHIIs from an observational and theoretical perspective. We start with single-dish line surveys toward a large sample obtaining their basic characteristics, and then perform detailed studies of selected sources using interferometers on smaller scales. These observations are accompanied by theoretical modeling of the chemical processes. Long-term goals are the chemical characterization of the evolutionary sequence in massive star formation, the development of chemical clocks, and the identification of molecules as astrophysical tools to study the physical processes during different evolutionary stages. Here we present an initial study of the reactive radical ethynyl (C_2H) combining single-dish and interferometer observations with chemical modeling. Although C_2H was previously observed in low-mass cores and photon-dominated regions (e.g., Millar & Freeman 1984; Jansen et al. 1995), so far it has not been systematically investigated in the framework of high-mass star formation.

2. OBSERVATIONS

The 21 massive star-forming regions were observed with the Atacama Pathfinder Experiment (APEX) in the $875 \mu m$ window in fall 2006. We observed 1 GHz from 338 to 339 GHz and 1 GHz in the image sideband from 349 to 350 GHz. The spectral resolution was 0.1 km s^{-1} , but we smoothed the data to $\sim 0.9 \text{ km s}^{-1}$. The average system temperatures were around 200 K; each source had on-source integration times between 5 and 16 minutes. The data were converted to main-beam temperatures with forward and beam efficiencies of 0.97 and 0.73, respectively (Belloche et al. 2006). The average 1σ rms was 0.4 K. The main spectral features of interest are the C_2H lines around 349.4 GHz with upper level excitation energies E_u/k of 42 K [line blends of $C_2H(4_{5,5}-3_{4,4})$ and $C_2H(4_{5,4}-3_{4,3})$ at 349.338 GHz, and $C_2H(4_{4,4}-3_{3,3})$ and $C_2H(4_{4,3}-3_{3,2})$ at 349.399 GHz]. The beam size was $\sim 18''$.

The original Submillimeter Array (SMA) C_2H data toward the HMPO 18089–1732 were first presented in Beuther et al. (2005a). There we used the compact and extended configurations resulting in good images for all spectral lines except for C_2H . For this project, we reworked these data using only the compact configuration. Because the C_2H emission is distributed on larger scales (see § 3), we were now able to derive a C_2H image. The integration range was from 32 to 35 km s^{-1} , and the achieved 1σ rms of the C_2H image was $450 \text{ mJy beam}^{-1}$. For more details on these observations see Beuther et al. (2005a).

3. RESULTS

The sources were selected to cover all evolutionary stages from IRDCs via HMPOs to UCHIIs. We derived our target list from the samples of Klein et al. (2005), Fontani et al. (2005), Hill et al. (2005), and Beltrán et al. (2006). Table 1 lists the observed sources, their coordinates, distances, and luminosities, and a first-order classification into the evolutionary subgroups IRDCs, HMPOs, and UCHIIs based on the previously available data. Although this classification is only based on a limited set of data, here we are just interested in general evolutionary trends. Hence, the division into the three main classes is sufficient.

Figure 1 presents sample spectra toward one source of each

TABLE 1
 SOURCE PARAMETERS

Name	Type	R.A. (J2000.0)	Decl. (J2000.0)	d (kpc)	L ($\log L_{\odot}$)	T_{mb} (K)	$\int T_{\text{mb}} dv$ (K km s $^{-1}$)	$\Delta v(\text{C}_2\text{H})$ (km s $^{-1}$)	Ref.
IRAS 07029	IRDC	07 05 11.1	-12 19 02	1.0	^a	0.21	0.52	2.4 \pm 0.3	1
IRAS 08477	IRDC	08 49 32.9	-44 10 47	1.8	^a	0.23	0.76	3.1 \pm 0.5	2, 3
IRAS 09014	IRDC	09 03 09.8	-47 48 28	1.3	^a	2, 3
IRAS 13039	IRDC	13 07 07.0	-61 24 47	2.4	^a	2, 3
IRAS 14000	IRDC	14 03 36.6	-61 18 28	5.6	^a	0.38	1.13	2.8 \pm 0.5	2, 3
IRAS 08211	HMPO	08 22 52.3	-42 07 57	1.7	3.5	0.38	0.85	2.1 \pm 0.2	2, 3
IRAS 08470	HMPO	08 48 47.9	-42 54 22	2.2	4.2	1.85	6.81	3.5 \pm 0.4	3
IRAS 08563	HMPO	08 58 12.5	-42 37 34	1.7	3.2	1.08	3.30	2.9 \pm 0.1	2, 3
IRAS 09131	HMPO	09 14 55.5	-47 36 13	1.7	3.4	0.23	0.50	2.1 \pm 0.3	2, 3
IRAS 09209	HMPO	09 22 34.6	-51 56 26	6.4	4.1	—	—	—	2, 3
IRAS 09578	HMPO	09 59 31.0	-57 03 45	1.7	3.9	0.21	0.64	2.8 \pm 0.4	3
IRAS 10123	HMPO	10 14 08.8	-57 42 12	0.9/3.0 ^b	3.4/4.4 ^b	0.17 ^c	0.46	2.5 \pm 0.4	2, 3
IRAS 10184	HMPO	10 20 14.7	-58 03 38	5.4	5.5	0.41	1.68	3.9 \pm 0.3	3
IRAS 10276	HMPO	10 29 30.1	-57 26 40	5.9	4.9	0.24 ^c	0.67	2.6 \pm 0.5	3
IRAS 10295	HMPO	10 31 28.3	-58 02 07	5.0	5.8	0.69	3.45	4.7 \pm 0.3	3
IRAS 10320	HMPO	10 33 56.4	-59 43 53	9.1	5.4	0.85	3.48	3.8 \pm 0.6	3
G294.97	UCHII	11 39 09.0	-63 28 38	1.3/5.8 ^b	3.9/5.3 ^b	0.31	0.78	2.3 \pm 0.4	4
G305.20	UCHII	13 11 12.3	-62 44 57	3.0/6.8 ^b	5.1/6.1 ^b	0.44	5.21	11.1 \pm 0.5	4
G305.37	UCHII	13 12 36.3	-62 33 39	3.0/6.8 ^b	^d	1.24	6.28	4.8 \pm 0.2	4
G305.561	UCHII	13 14 25.8	-62 44 32	4.0	5.1	0.94	4.71	4.7 \pm 0.6	4, 5
IRAS 14416	UCHII	14 45 22.0	-59 49 39	2.8	5.1	1.24	6.19	4.7 \pm 0.6	6

NOTE.—Units of right ascension are hours, minutes, and seconds, and units of declination are degrees, arcminutes, and arcseconds.

^a Since the IRDCs are by default not detected at short wavelengths, they are not IRAS sources and we cannot derive a luminosity.

^b Near and far distances and corresponding luminosities.

^c For these sources we list the parameters of the C₂H line blend at 349.338 GHz; for all other sources it is the C₂H line at 349.399 GHz.

^d No IRAS counterpart, hence no luminosity estimate.

REFERENCES.—(1) Klein et al. 2005; (2) Fontani et al. 2005; (3) Beltrán et al. 2006; (4) Hill et al. 2005; (5) Faúndez et al. 2004; (6) Vig et al. 2007.

evolutionary group. While we see several CH₃OH lines as well as SO₂ and H₂CS toward some of the HMPOs and UCHIIIs but not toward the IRDCs, the surprising result of this comparison is the presence of the C₂H lines around 349.4 GHz toward all source types from young IRDCs via the HMPOs to evolved UCHIIIs. Table 1 lists the peak brightness temperatures, the integrated intensities, and the FWHM line widths of the C₂H line blend at 349.399 GHz. The separation of the two lines of 1.375 MHz already corresponds to a line width of 1.2 km s⁻¹. We have three C₂H nondetections (2 IRDCs and 1 HMPO), however, with no clear trend with respect to the distances or the luminosities (the latter comparison is only possible for the HMPOs). While IRDCs are on average colder than more evolved sources and have lower brightness temperatures, the nondetections are more probable due to the relatively low sensitivity of the short observations (§ 2). Hence, the data indicate that the C₂H lines are detected independent of the evolutionary stage of the sources in contrast to the situation with other molecules. When comparing the line widths between the different subgroups, one finds only a marginal difference between the IRDCs and the HMPOs (the average Δv values of the two groups are 2.8 and 3.1 km s⁻¹). However, the UCHIIIs exhibit significantly broader line widths with an average value of 5.5 km s⁻¹.

Intrigued by this finding, we wanted to understand the C₂H spatial structure during the different evolutionary stages. Therefore, we went back to a data set obtained with the SMA toward the hypercompact HII region IRAS 18089–1732 with a much higher spatial resolution of $\sim 1''$ (Beuther et al. 2005a). Albeit this hypercompact HII region belongs to the class of HMPOs, it is already in a relatively evolved stage and has formed a hot core with a rich molecular spectrum. Beuther et al. (2005a) showed the spectral detection of the C₂H lines toward this source, but they did not present any spatially resolved images. To recover

large-scale structure, we restricted the data to those from the compact SMA configuration (§ 2). With this refinement, we were able to produce a spatially resolved C₂H map of the line blend at 349.338 GHz with an angular resolution of $2.9'' \times 1.4''$ (corresponding to an average linear resolution of 7700 AU at the given distance of 3.6 kpc). Figure 2 presents the integrated C₂H emission with a contour overlay of the 860 μm continuum source outlining the position of the massive protostar. In contrast to almost all other molecular lines that peak along with the dust continuum (Beuther et al. 2005a), the C₂H emission surrounds the continuum peak in a shell-like fashion.

4. DISCUSSION AND CONCLUSIONS

To understand the observations, we conducted a simple chemical modeling of massive star-forming regions. A 1D cloud model with a mass of $1200 M_{\odot}$, an outer radius of 0.36 pc, and a power-law density profile ($\rho \propto r^p$ with $p = -1.5$) is the initially assumed configuration. Three cases are studied: a cold isothermal cloud with (1) $T = 10$ K and (2) $T = 50$ K, and (3) a warm model with a temperature profile $T \propto r^q$ with $q = -0.4$ and a temperature at the outer radius of 44 K. The cloud is illuminated by the interstellar UV radiation field (IRSF; Draine 1978) and by cosmic ray particles (CRPs). The IRSF attenuation by single-sized 0.1 μm silicate grains at a given radius is calculated in a plane-parallel geometry following van Dishoeck (1988). The CRP ionization rate is assumed to be $1.3 \times 10^{-17} \text{ s}^{-1}$ (Spitzer & Tomasko 1968). The gas-grain chemical model by Vasyunin et al. (2008) with the desorption energies and surface reactions from Garrod et al. (2007) is used. Gas-phase reaction rates are taken from RATE 06 (Woodall et al. 2007); initial abundances were adopted from the “low metal” set of Lee et al. (1998).

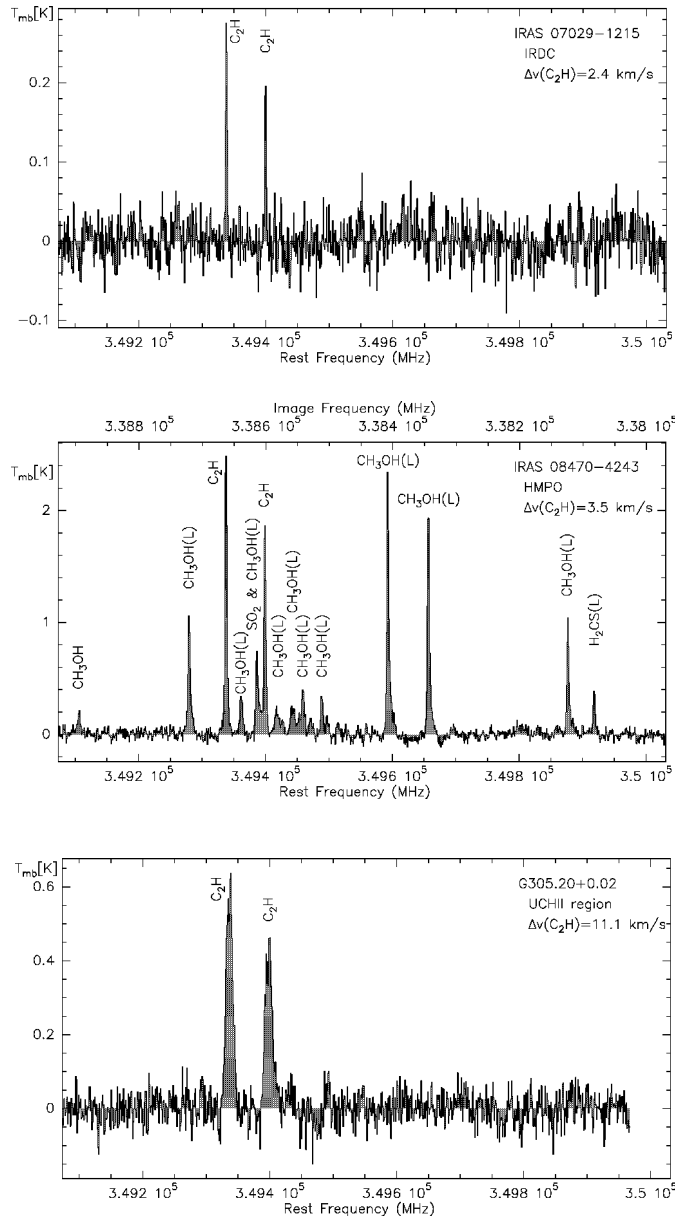


FIG. 1.—Sample spectra obtained with APEX in a double-sideband mode. The spectra cover 1 GHz of data around 349.5 GHz and 1 GHz around 338.5 GHz. All spectral lines are labeled; lines in the lower sideband are marked with “(L)”. The top panel shows an IRDC example, the middle panel a typical HMPO/hot core, and the bottom panel a UCHII region. The C₂H line widths are indicated in each panel.

Figure 3 presents the C₂H abundances for the three models at two different time steps: (1) 100 yr, and (2) in a more evolved stage after 5×10^4 yr. The C₂H abundance is high toward the core center right from the beginning of the evolution, similar to previous models (e.g., Millar & Nejad 1985; Herbst & Leung 1986; Turner et al. 1999). During the evolution, the C₂H abundance stays approximately constant at the outer core edges, whereas it decreases by more than 3 orders of magnitude in the center, except for the cold $T = 10$ K model. The C₂H abundance profiles for all three models show similar behavior.

The chemical evolution of ethynyl is determined by relative removal rates of carbon and oxygen atoms or ions into molecules such as CO, OH, and H₂O. Light ionized hydrocarbons CH_{*n*}⁺ ($n = 2-5$) are quickly formed by radiative association of C⁺ with H₂ and hydrogen addition reactions: C⁺ → CH₂⁺ → CH₃⁺ →

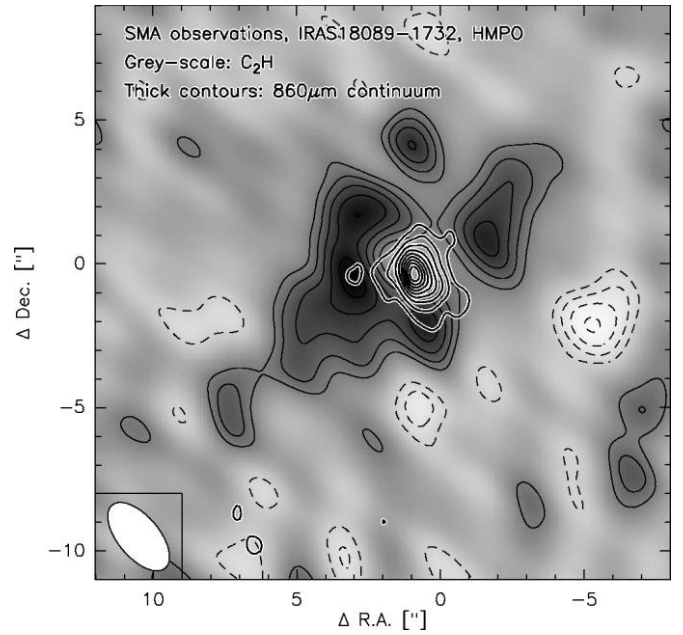


FIG. 2.—Gray scale shows the integrated emission (from 32 to 35 km s⁻¹) of the line blend of C₂H(4_{5,5}-3_{4,4}) and C₂H(4_{3,4}-3_{4,3}) around 349.338 GHz obtained with the Submillimeter Array using only the compact configuration data (Beuther et al. 2005a). The resulting synthesized beam is shown at the lower left corner (2.9'' × 1.4''). The C₂H emission is presented in gray scale with thin contours (dashed contours indicate negative features), and the 860 μm continuum peak is shown in thick contours. The C₂H emission starts at the 2 σ level and continues in 1 σ steps with the 1 σ level of 450 mJy beam⁻¹. The 860 μm emission is contoured from 10% to 90% (steps of 10%) of the peak emission of 1.4 Jy beam⁻¹.

CH₅⁺. The protonated methane reacts with electrons, CO, C, OH, and more complex species at later stages and forms methane. The CH₄ molecules undergo reactive collisions with C⁺, producing C₂H₂⁺ and C₂H₃⁺. An alternative way to produce C₂H₂⁺ is the dissociative recombination of CH₅⁺ into CH₃, followed by reactions with C⁺. Finally, C₂H₂⁺ and C₂H₃⁺ dissociatively recombine into CH, C₂H, and C₂H₂. The major removal for C₂H is either the direct neutral-neutral reaction with O that forms CO, or the same reaction but with heavier carbon chain ions that are formed from C₂H by subsequent insertion of carbon. At later times, depletion and gas-phase reactions with more complex species may enter into this cycle. At the cloud edge the interstellar UV radiation instantaneously dissociates CO despite its self-shielding, reenriching the gas with elemental carbon.

The transformation of C₂H into CO and other species proceeds efficiently in dense regions, in particular in the “warm” model where endothermic reactions result in rich molecular complexity of the gas (see Fig. 3). In contrast, in the “cold” 10 K model gas-grain interactions and surface reactions become important. As a result, a large fraction of oxygen is locked in water ice that is hard to desorb ($E_{\text{des}} \sim 5500$ K), while half of the elemental carbon goes to volatile methane ice ($E_{\text{des}} \sim 1300$ K). Upon CRP heating of dust grains, this leads to a much higher gas-phase abundance of C₂H in the cloud core for the cold model compared to the warm model. The effect is not that strong for less dense regions at larger radii from the center.

Since the C₂H emission is anticorrelated with the dust continuum emission in the case of IRAS 18089-1732 (Fig. 2), we do not have the H₂ column densities to quantitatively compare the abundance profiles of IRAS 18089-1732 with our model. However, data and model allow a qualitative comparison of the spatial structures. Estimating an exact evolutionary

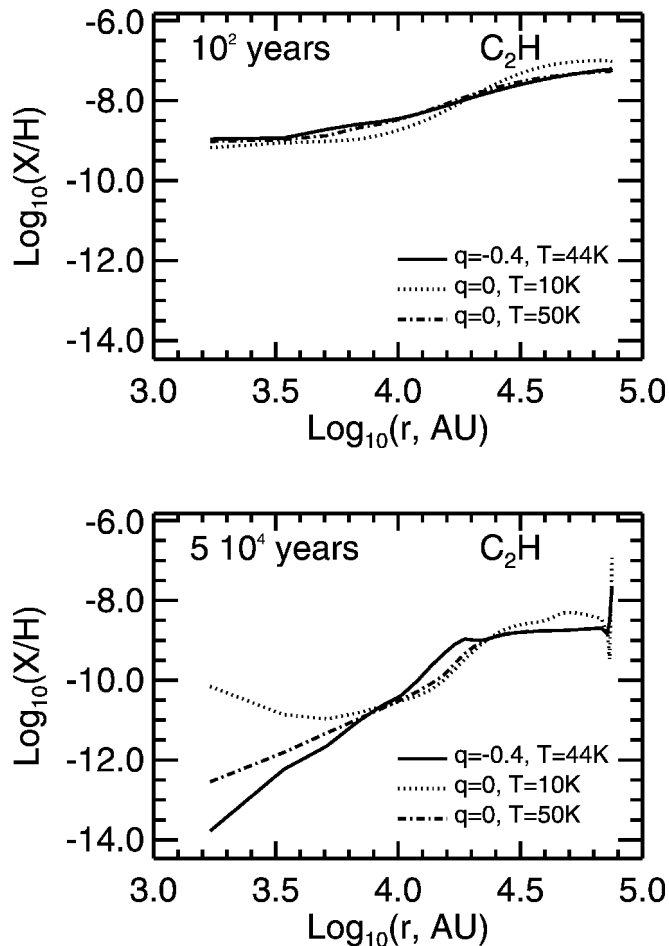


FIG. 3.—*Top*: Radial profiles of the C_2H abundance for the three cloud models at early times, $t \lesssim 100$ yr. *Bottom*: The same, but for the later time step of 5×10^4 yr. The parameter q denotes the exponent of the assumed temperature distribution (see also main text).

time for IRAS 18089–1732 is hardly possible, but based on the strong molecular line emission, its high central gas temperatures, and the observed outflow-disk system (Beuther et al. 2004a, 2004b, 2005a), an approximate age of 5×10^4 yr appears reasonable. Although dynamical and chemical times are not necessarily exactly the same, in high-mass star for-

mation they should not differ too much: following the models by McKee & Tan (2003) or Krumholz et al. (2007) the luminosity rises strongly right from the onset of collapse, which can be considered as a starting point for the chemical evolution. At the same time disks and outflows evolve, which should hence have similar timescales. The diameter of the shell-like C_2H structure in IRAS 18089–1732 is $\sim 5''$ (Fig. 2), or ~ 9000 AU in radius at the given distance of 3.6 kpc. This value is well matched by the modeled region with decreased C_2H abundance (Fig. 3). Although in principle optical depths and/or excitation effects could mimic the C_2H morphology, we consider this as unlikely because the other observed molecules with many different transitions all peak toward the central submillimeter continuum emission in IRAS 18089–1732 (Beuther et al. 2005a). Since C_2H is the only exception in that rich data set, chemical effects appear the more plausible explanation.

The fact that we see C_2H at the earliest and the later evolutionary stages can be explained by the reactive nature of C_2H : it is produced quickly early on and gets replenished at the core edges by the UV photodissociation of CO. The inner “chemical” hole observed toward IRAS 18089–1732 can be explained by C_2H being consumed in the chemical network, forming CO and more complex molecules such as larger carbon-hydrogen complexes, and/or depletion.

The data show that C_2H is not suited to investigate the central gas cores in more evolved sources; however, our analysis indicates that C_2H may be a suitable tracer of the earliest stages of (massive) star formation, like N_2H^+ or NH_3 (e.g., Bergin et al. 2002; Tafalla et al. 2004; Beuther et al. 2005b; Pillai et al. 2006). While a spatial analysis of the line emission will give insights into the kinematics of the gas and also the evolutionary stage from chemical models, multiple C_2H lines will even allow a temperature characterization. With its lowest $J = 1-0$ transitions around 87 GHz, C_2H has easily accessible spectral lines in several bands between 3 mm and 850 μm . Furthermore, even the 349 GHz lines presented here still have relatively low upper level excitation energies ($E_u/k \sim 42$ K), hence allowing the study of cold cores even at submillimeter wavelengths. This prediction can further be proved via high spectral and spatial resolution observations of different C_2H lines toward young IRDCs.

H. B. acknowledges financial support by the Emmy-Noether-Programm of the Deutsche Forschungsgemeinschaft (DFG; grant BE2578).

REFERENCES

- Belloche, A., et al. 2006, *A&A*, 454, L51
 Beltrán, M. T., et al. 2006, *A&A*, 447, 221
 Bergin, E. A., Alves, J., Huard, T., & Lada, C. J. 2002, *ApJ*, 570, L101
 Bergin, E. A., & Langer, W. D. 1997, *ApJ*, 486, 316
 Beuther, H., Churchwell, E. B., McKee, C. F., & Tan, J. C. 2007, in *Protostars and Planets V*, ed. B. Reipurth et al. (Tucson: Univ. Arizona Press), 165
 Beuther, H., Zhang, Q., Sridharan, T. K., & Chen, Y. 2005a, *ApJ*, 628, 800
 Beuther, H., et al. 2004a, *ApJ*, 616, L19
 ———. 2004b, *ApJ*, 616, L23
 ———. 2005b, *ApJ*, 632, 355
 Bisschop, S. E., et al. 2007, *A&A*, 465, 913
 Comito, C., et al. 2005, *ApJS*, 156, 127
 Draine, B. T. 1978, *ApJS*, 36, 595
 Dutrey, A., Guilloteau, S., & Guelin, M. 1997, *A&A*, 317, L55
 Faúndez, S., et al. 2004, *A&A*, 426, 97
 Fontani, F., et al. 2005, *A&A*, 432, 921
 Garrod, R. T., Wakelam, V., & Herbst, E. 2007, *A&A*, 467, 1103
 Hatchell, J., et al. 1998, *A&AS*, 133, 29
 Herbst, E., & Leung, C. M. 1986, *MNRAS*, 222, 689
 Hill, T., et al. 2005, *MNRAS*, 363, 405
 Jansen, D. J., et al. 1995, *A&A*, 302, 223
 Jørgensen, J. K., et al. 2007, *ApJ*, 659, 479
 Klein, R., et al. 2005, *ApJS*, 161, 361
 Krumholz, M. R., Klein, R. I., & McKee, C. F. 2007, *ApJ*, 656, 959
 Lee, H.-H., et al. 1998, *A&A*, 334, 1047
 McKee, C. F., & Tan, J. C. 2003, *ApJ*, 585, 850
 Millar, T. J., & Freeman, A. 1984, *MNRAS*, 207, 405
 Millar, T. J., & Nejad, L. A. M. 1985, *MNRAS*, 217, 507
 Pavlyuchenkov, Y., et al. 2006, *ApJ*, 645, 1212
 Pillai, T., Wyrowski, F., Carey, S. J., & Menten, K. M. 2006, *A&A*, 450, 569
 Schilke, P., et al. 1997, *ApJS*, 108, 301
 Spitzer, L. J., & Tomasko, M. G. 1968, *ApJ*, 152, 971
 Tafalla, M., et al. 2004, *A&A*, 416, 191
 Turner, B. E., Terzieva, R., & Herbst, E. 1999, *ApJ*, 518, 699
 van Dishoeck, E. F. 1988, in *Rate Coefficients in Astrochemistry*, ed. T. J. Millar et al. (Dordrecht: Kluwer), 49
 Vasyunin, A. I., et al. 2008, *ApJ*, 672, 629
 Vig, S., Ghosh, S. K., Ojha, D. K., & Verma, R. P. 2007, *A&A*, 463, 175
 Woodall, J., et al. 2007, *A&A*, 466, 1197